sciendo
Power Electronics and Drives
Volume 9(44), 2024 DOI: 10.2478/pead-2024-0008

A Novel Proportional Multi-Resonant Current Controller Strategy for Reduced DC Voltage fed D-STATCOM with Internal LCL Resonance Damping

Research paper

Guddy Satpathy, Dipankar De*

School of Electrical Sciences (Electrical Engineering), IIT Bhubaneswar, Argul Campus, Jatni, Odisha-752050, India

Received: 24 October 2023; Accepted: 31 January 2024

Abstract: This work focuses on a new topology-control-based D-STATCOM solution with reduced DC bus voltage requirement and with an excellent grid side performance. The proposed solution consists of a main inverter and auxiliary inverter along with a transformer and LCL filter network to achieve the required DC bus reduction. A new controller structure with two proportional-multi resonant controller for the converters with only one of the inductors current as a controlled variable ensures the active damping of the LCL resonance. The power circuit configuration assists the controller to generate a difference in the modulation signal due to non-equal gains in two controllers and helps to achieve the resonance damping without capacitor current sensor. Hence, the corresponding capacitor current sensor can be eliminated. The converter operates for any point of common coupling (PCC) loading conditions and the performance of the controller is immune to the grid impedance variation. A detailed stability study is carried out for the proposed controller. The proposed controller can achieve a very fast dynamic response with an excellent stability margin. The proposed solution is verified through simulation studies and through a scaled-down experimental prototype.

Keywords: *active filtering • D-STATCOM • proportional resonant controller • LCL filter*

1. Introduction

With the advent of recent technology, power quality has become a major concern. Active filtering and D-STATCOM are two solutions from the existing few viable solutions used to tackle the problem of power quality (Barva and Joshi, 2022; Gajjar and Zaveri, 2018; Nikam and Kalkhambkar, 2018; Rosso et al., 2021; Park et al., 1999). Operating the active filter at reduced DC bus voltage has its own advantages like avoiding the addition of extra PVs in series. The disadvantage of connecting a large number of PVs in series is that if one array suffers from partial shading then it is difficult to control optimum power generation by MPPT (Olalla et al., 2013). The number of series-connected cells is limited to form just adequate amount of voltage DC needed (Gao et al., 2009) before boosting for grid integration. Several topologies are reported in the literature for integrating a low voltage fed D-STATCOM to the grid. For high-power applications, commonly multi-level inverters (MLI) are used. However, they suffer from drawbacks like high component counts, large number of DC supplies, high system cost and losses and loss of system reliability (Naidu et al., 2021; Pilli et al., 2019). The neutral point capacitor type and flying capacitor type MLI have a single DC source, but the voltage imbalance problem is severe in these configuration (Khenar et al., 2018; Mondol et al., 2022; Sadanala et al., 2021).

* Email: dipankar@iitbbs.ac.in

The advantages associated with reduced DC bus power converter systems are:

- It is possible to select Low-voltage semiconductor devices. With the low breakdown voltage of the device ON state losses are lower.
- Additional boost stage can be eliminated in the case of PV-fed inverters and hence higher efficiency.
- Reduced DC bus helps to reduce the grid side filter size.
- From generated noise point of view, the reduced DC bus system is preferred.
- From a converter design point of view, lower DC bus voltage helps to achieve improved component packaging and improved power density.

Challenges associated with the Reduced DC bus voltage:

- The reduced bus voltage should be sufficient for grid connection. If the voltage falls below a certain level, the grid current control will be lost. The amplitude of the voltage depends on the topology selected.
- The capacitance requirement of the reduced DC voltage system is generally higher as stored energy is proportional to the square of the DC bus voltage. During transients, the closed loop controller along with selected DC bus capacitance should ensure minimum deviation in the DC voltage.
- For a given power rating, reduced DC bus implies high current of the semiconductor switches; this can be achieved via higher rating devices or through parallel paths.

Figure 1 shows a configuration where the grid voltage is stepped down to a desired voltage level by transformer. In this case, the transformer rating is high (with rated voltage and current). The current rating of the semiconductor devices is more than the actual current rating on the grid side due to transformer action. Figure 2 gives another circuit that eliminates the direct transformer and it is replaced by inserting a capacitor along with filter inductor (Satpathy et al., 2017). This helps to reduce the voltage across the inverter and hence the ratings of the switches. However, it suffers from the drawback that certain reactive current must be injected irrespective of the load present at the point of common coupling (PCC). This leads to non-unity power factor at the grid side and the power factor varies as the load at PCC varies.

One of the possible configurations to reduce the DC bus requirement with reduced transformer rating is shown in Figure 3. In this configuration the DC bus voltage requirement can be reduced by adjusting transformer turns ratio. It can be observed that the power circuit contains two inverters namely, main and auxiliary inverters connected through transformer. With grid inductance, the converter has LCL filter at the output side. However, the topology has a drawback in terms of control which is described in the next section. Hence, a slight variation of this topology is proposed in this paper.

Several attempts have been made to dampen out the LCL resonance oscillations in grid-connected inverters. One such possibility is by passive damping (Albatran et al., 2018; Pea et al., 2020; Wu et al., 2013) that is, placing

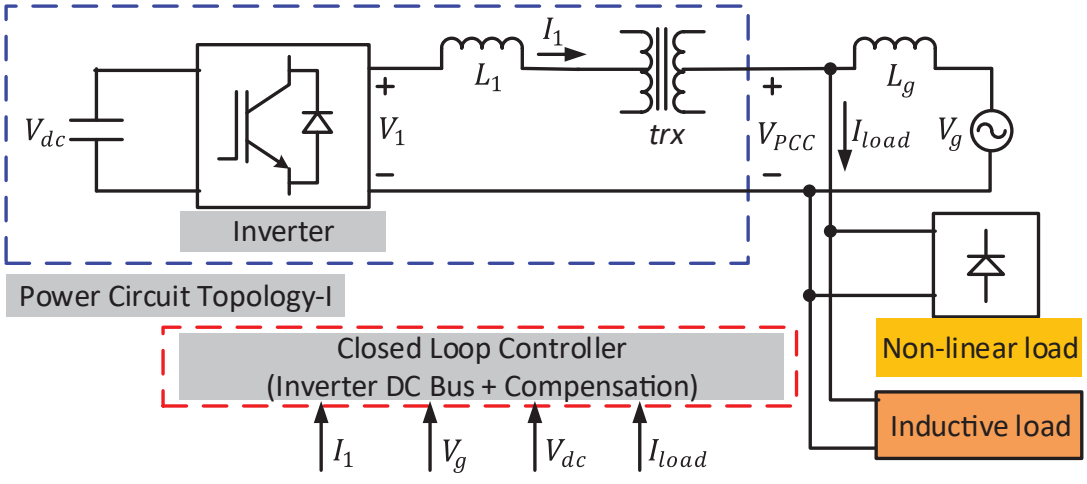

Fig. 1. Direct integration of conventional grid-connected inverter with transformer.

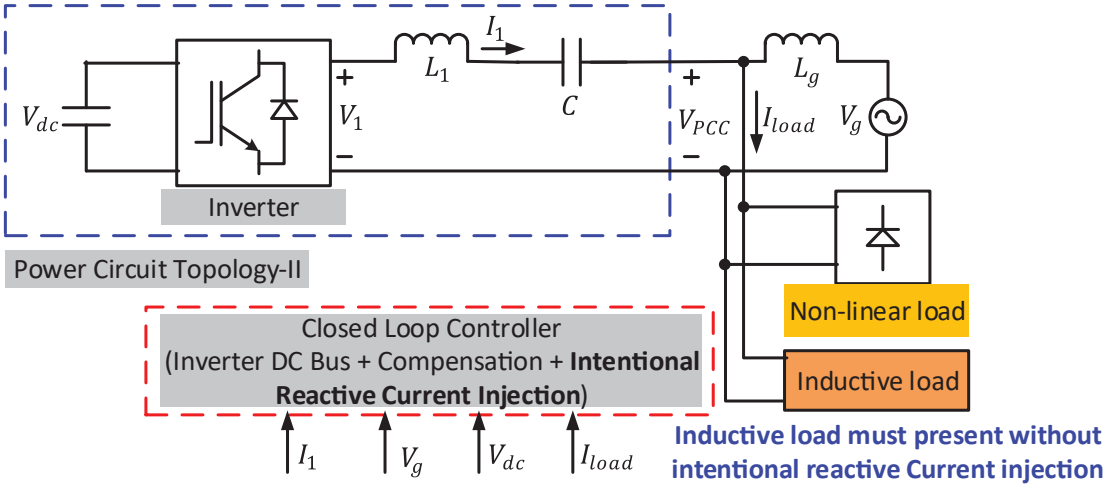

Fig. 2. Configuration with intentional reactive current injection for DC voltage reduction (Satpathy et al., 2017).

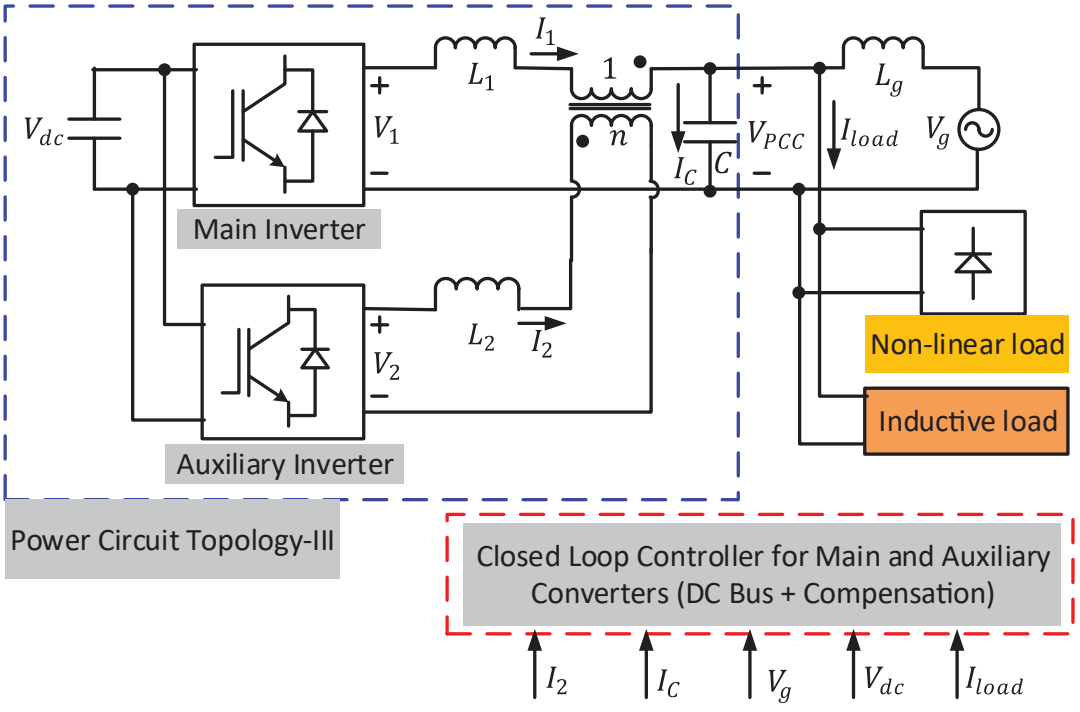

Fig. 3. Alternate topology for DC voltage reduction.

a resistor in various possible combinations with L and C. This method is lossy in nature and the efficiency of the overall system reduces. Hence, to overcome this drawback, the active damping method was introduced. (Pan et al., 2014; Tang et al., 2012) give a two-control loop in which the outer loop is used for current control and the inner loop senses the capacitor current or capacitor voltage for the purpose of active damping. The system needs an additional sensor for sensing the capacitor current or voltage (Gonzalez et al., 2021). Subsequently the two-control loop was replaced by single loop that features sensing of just inverter/grid current for both current control and damping purpose. If inverter current is measured and controlled, the LCL resonating frequency should be <1/6th of control frequency otherwise the system would not be able to damp out the oscillations, and this results in poor harmonic filtering (Jeong et al., 2010; Zhang et al., 2006). On the other hand, if grid current is sensed and controlled then the LCL resonating frequency should be >1/6th of the control frequency (Almaguer et al., 2019;

Parker et al., 2014; Yin et al., 2013). Further investigation in single control loop shows that a high pass filter, lead lag compensator or notch filter cascaded with the current control (Buyuk et al., 2018; Pea-Alzola et al., 2014; Yao et al., 2017) may help damp out the oscillations accounted for the deviation in resonant frequency, but they too are sensitive to system parameter variations (Akhavan et al., 2021; Wang et al., 2016).

This paper proposes a new method of voltage reduction as shown in Figure 4. Here, no such intentional injection of current (as in Figure 2) is required. A transformer aids the process though not connected directly across the grid and inverter (as in Figure 1) but connected in series with the system.

Moreover, from the control and feedback sensing point of view, the proposed configuration exhibits improved performance compared to that shown in Figure 3. In order to achieve effective damping of the oscillations the proposed configuration uses both the inverters each fed by separate modulation signals. The two modulation signals are obtained by the proposed controller to provide active damping of the LCL oscillations along with supplying the compensating current without using any additional sensors as in case of capacitor voltage or current feedback-based damping.

In this paper, a detailed study has been carried out to provide stable operation with different combinations of the series and shunt side inductance values. A novel controller strategy is proposed which meets all the requirements

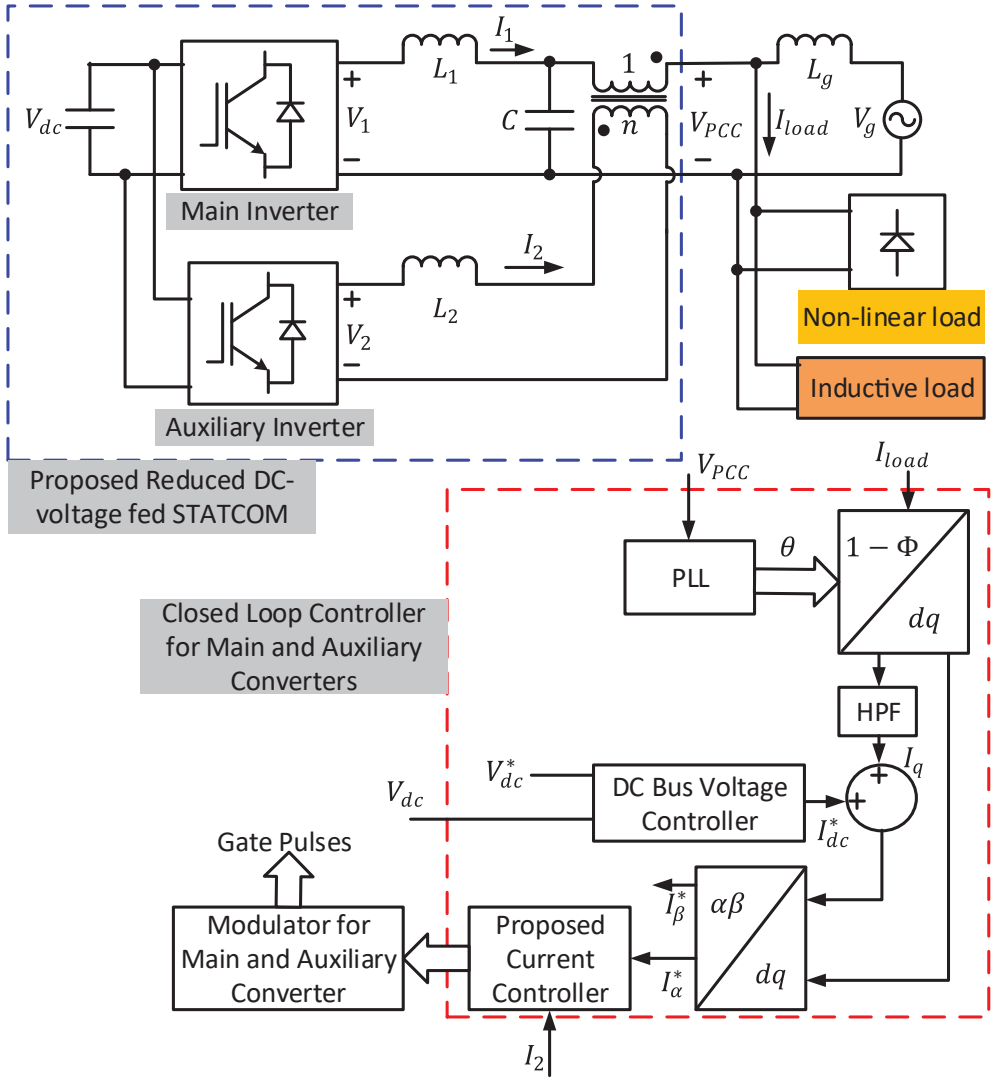

Fig. 4. Proposed topology for DC voltage reduction along with improved control of LCL filter.

such as minimal sensors (removal of active damping), better performance at reduced inductances, cost-effective and fast controller action. In summary, the contribution of the paper is as follows:

- A novel reduced DC bus fed D-STATCOM topology with reduced transformer rating.
- A closed-loop solution along with power circuit architecture to achieve resonance damping of LCL resonance using only inductor current feedback.
- The proposed solution provides stable performance with grid and converter inductance variation.

This paper is organised as follows. Section 2 gives the description and the control structure of proposed topology. A detailed analysis of the proposed controller is laid out and compared with the conventional single controller strategy. Section 3 gives the simulation results. Section 4 shows the results obtained by hardware testing and finally, Section 5 gives the conclusion of the work.

2. Description of Proposed Power Circuit and Controller and Controller Design Considerations

A brief comparison of different topologies is given in Table 1. The topologies with series capacitor with inductor have very high operating efficiency however, the performances of these topologies are PCC load dependent with intentional current injection and variable power factor at the grid side. However, they suffer from low reliability irrespective of lower component count due to the presence series capacitor (with high low frequency ripple current through it). The topologies with transformer have additional losses and very high efficiencies cannot be achieved. The topology under consideration in this paper has nearly 50% volume/size compared to direct transformer integrated cases.

The rating of the transformer can be reduced as compared to that in Figure 1. By adjusting the turns ratio of the transformer, a trade-off between the DC voltage reduction and rating of the transformer can be achieved. This trade of is shown in Figure 5. Its rating depends upon the amount by which inverter voltage is to be reduced and the load current that is to be compensated. The DC bus voltage can be calculated by referring to Figure 4 and is given by Eq. (1) ignoring the drops in the inductors. The effect of the inductor drops can be incorporated in the maximum value of the modulation index.

$$V_1 = V_g - \frac{V_2}{n}$$

Topology	Reliability	Operating efficiency	T-Size	Initial cost	Component count*(S/L/C/T)	PCC load dependent?	Phase	Vdc/Vg ratio	Input filter
Bhattacharya et al. (2012)	Low	Excellent	n/a	Medium	8/5/5/0	Yes	3	Low	Simple
Luo et al. (2012)	Medium	Average	100%	High	6/21/15/3	No	3	Low	Hybrid
Srianthumrong and Akagi (2002)	Low	Excellent	n/a	Low	6/3/3/0	Yes	3	Medium	Simple
Kim and Enjeti (2002)	High	Good	100%	Medium	12/6/3/3	No	3	Low	Simple
Rahmani et al. (2014)	Low	Excellent	n/a	Low	6/6/3/0	Yes	3	Medium	Hybrid
Luo et al. (2009)	High	Good	100%	Medium	6/12/15/3	No	3	Low	Hybrid
Tangtheerajaroonwong et al. (2007)	Low	Excellent	n/a	Medium	12/3/3/0	Yes	3	Medium	Simple
Johnsana and Kumar (2022)	High	Excellent	n/a	Low	4/2/1/0	No	1	High	Simple
Behera et al. (2021)	Medium	Good	100%	High	12/3/0/9	No	3	Low	Simple
Topology in this paper	High	Good	50%	Medium	8/2/1/1	No	1	Medium	Simple

*Excluding the DC link Capacitor, S-Switches, L-inductors, C-Capacitors, T-Transformers, T-Size: Size of the transformer in terms of converter rating.

PCC, point of common coupling.

Table 1. Comparison with different topologies.

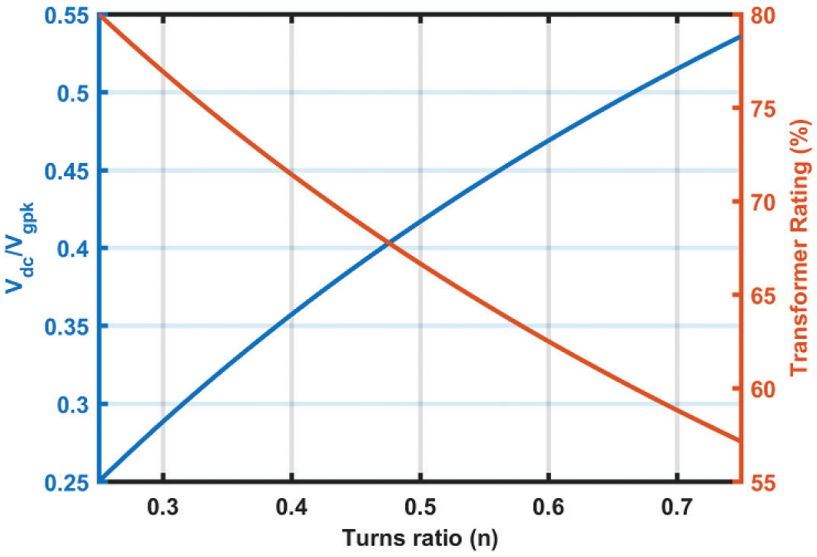

Fig. 5. Trade-off study between the DC bus voltage (in relative to peak grid voltage) and transformer rating with its turns ratio variation.

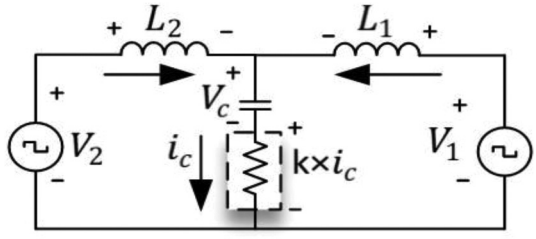

Fig. 6. Equivalent circuit with virtual resistance.

It can be observed from Figure 5 that with increased turns ratio, the required transformer rating reduces from that in Figure 1 and the minimum required DC bus voltage increases. In Figure 5, the DC bus voltage is expressed relative to the peak grid voltage.

The proposed closed-loop control of the reduced DC fed active filter is explained in this section. Figure 6 shows a general equivalent circuit with a virtual resistance that causes active damping of the oscillations caused by LCL filter where V_1 and V_2 are the two-excitation inputs to the filter network to emulate a virtual resistance in series with the capacitor to achieve loss-less damping. Eq. (1) governs the circuit operation in Figure 6.

$$V_1 - L_1\frac{di_1}{dt} - ki_c - V_c = 0$$

$$V_2 + V_c - ki_c - L_2\frac{di_2}{dt} = 0 \tag{1}$$

where,

$$V_1 = \frac{m_{sh}V_{dc}}{n}$$

$$V_2 = m_{se}V_{dc}$$

$$L_1 = \frac{L_{series}}{n^2}$$

$$L_2 = L_{series} \tag{2}$$

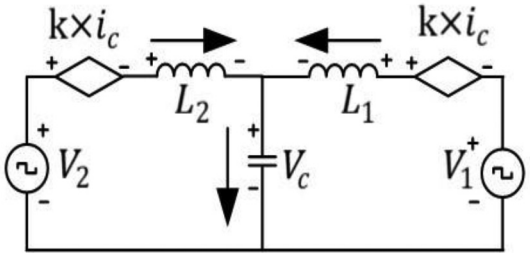

Fig. 7. Equivalent circuit of Eq. (1).

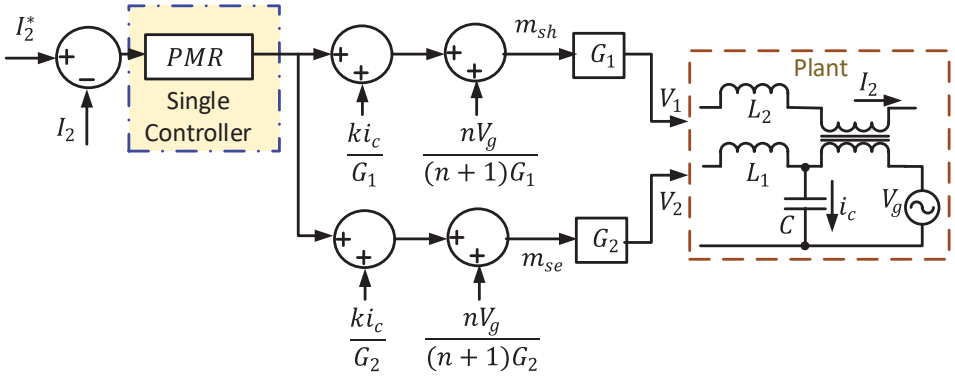

Fig. 8. Single current controller with active damping method. PMR, proportional multi resonant.

m_{sh} is the modulation signal given to the main inverter whereas m_{se} is the modulation signal given to the auxiliary inverter. Figure 7 shows the equivalent circuit diagram representing that in Figure 6 with two dependent sources separated which assists in achieving active damping. This equivalent circuit can be realised in the closed loop form conventionally. Figure 8 shows the control strategy with capacitor current feedback in the modulation of both inverters and with a single current controller. The controller is selected in this case proportional plus multi-resonant controller to ensure high accuracy of harmonic filtering and capacitor current feedback ensures active damping. It can be noted the current controller in Figure 8 requires two current feedbacks.

Figure 9 shows the performance of this single controller with capacitive current-based active damping. It can be observed from Figure 9 that a phase margin as good as 60° can be achieved around a bandwidth of 1 kHz. It works well with all values of inductances as can be seen in Figure 10. Here, *x* denotes the factor by which the designed value of series inductance is varied, and *a* is the controller gains as explained in the next section.

Figure 11 shows the structure of the proposed controller without the capacitor current feedback, that is, k = 0. In this controller, the current feedback is compared with the reference current (I_2^* in Figure 11 and it is same as I_α^* in Figure 4) to generate the error signal. The error signal is processed by two different controllers to generate the modulation signals for the main and auxiliary converters. When the converters are fed with different modulations, the system damped out the oscillations satisfactorily.

The open loop transfer function for the current loop can be expressed as Eq. (3).

$$\frac{I_2(s)}{e(s)} = \frac{P_2G_2 + \dfrac{P_1G_1n}{1+s^2L_1C}}{sL_2 + \dfrac{sn^2L_1}{1+s^2L_1C}} \tag{3}$$

where P_1 and P_2 are proportional multi resonant (PMR) controllers,

$$PMR = K_p + \sum_{m=1}^{9} \frac{K_i \times 2\zeta(m\omega)s}{\left[s^2 + 2\zeta(m\omega)s + (m\omega)^2\right]}$$

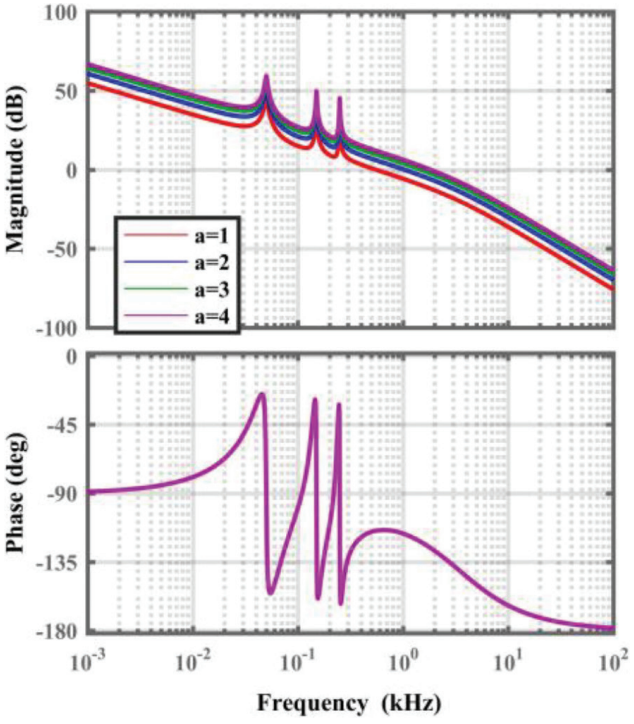

Fig. 9. Performance of system using single controller with damping ($a = b$).

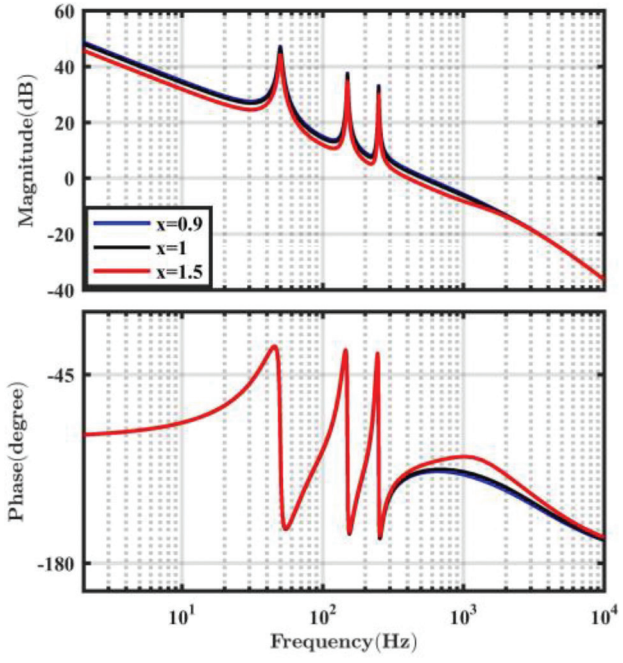

Fig. 10. Performance of system using single controller with damping and various inductances.

where $K_p = a$ for shunt controller and $K_p = b$ for series controller and K_1 to $K_9 = 20K_p$. Figure 11 can be reduced to single controller if a and b share the same values whereas in the proposed controller, they share different values. Figure 12 shows the operation of single controller and proposed controller systems. It can be observed that both

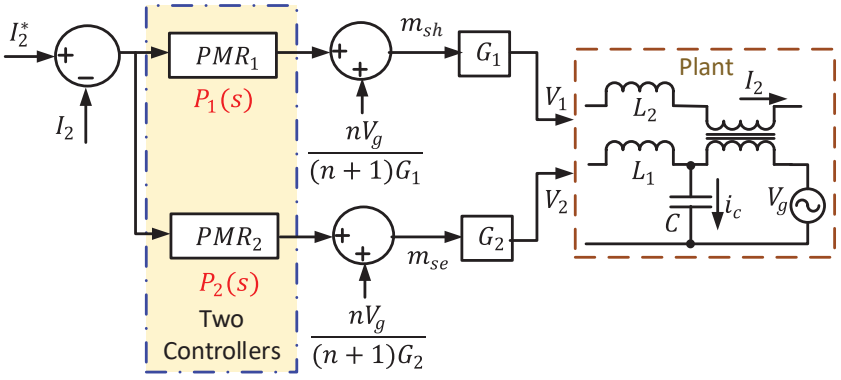

Fig. 11. Proposed controller with inherent active damping (no capacitor current feedback). PMR, proportional multi resonant.

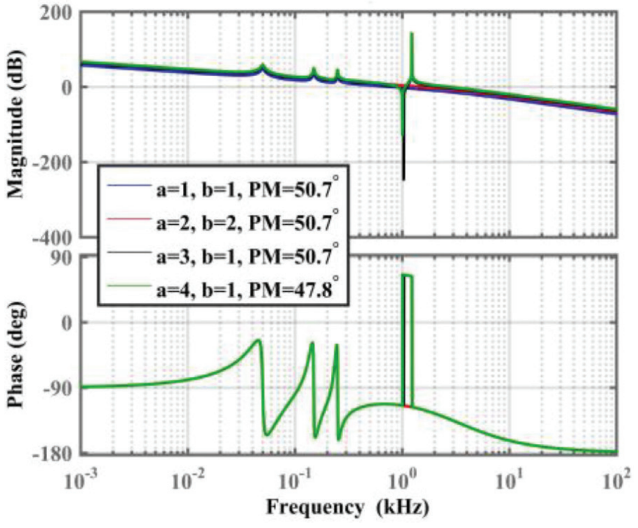

Fig. 12. Closed loop response for designed inductance by single and proposed controller.

Controller	Switching frequency	Control complexity	Response time	Steady state error in active filtering	Capacitor current feedback requirement for active damping
Hysteresis current control	Varying	Low	Fast	High	Yes
Quasi-proportional resonant control	Constant	Medium	Slow	High	Yes
Deadbeat current control	Constant	Low	Fast	Medium	Yes
Second order sliding mode control	Constant	Medium	Fast	Medium	Yes
Vector proportional-integral controller	Constant	High	Fast	Low	Yes
Model predictive control	Varying	Low	Fast	Medium	Yes
Proposed controller	Constant	Low	Fast	Low	No

Table 2. Comparison with different control techniques (Hong et al., 2022) for the power circuit considered in this paper.

the controllers are properly functioning for designed value of series and shunt inductances. Table 5 gives the values of the controller parameters. The values of phase margin are indicated for both controllers. The pole zero plots of the closed-loop transfer functions of the system with increased grid inductance by 1 mH using single controller and proposed controller are shown in Figures 13 and 14, respectively. The movement of closed loop poles on increasing the gain of the controller is observed. It can be seen in Figure 13 that the closed loop poles for the single controller without capacitor current feedback lie on the imaginary axis of the complex s-plane and move towards the right half

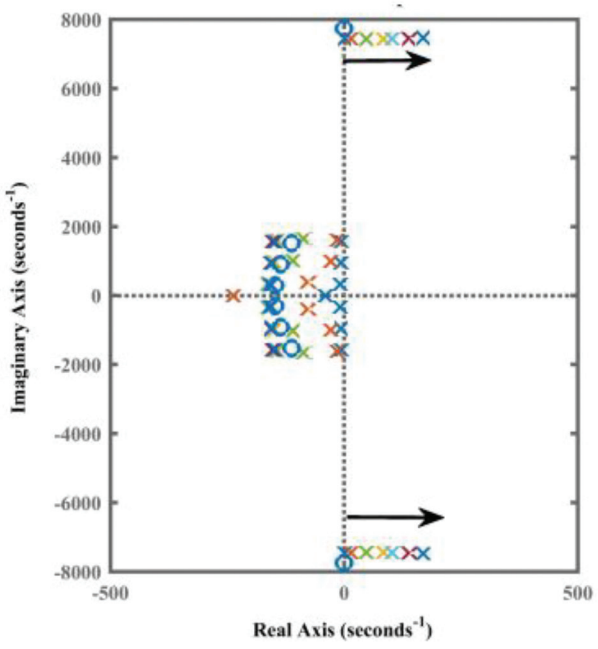

Fig. 13. Pole Zero plot depicting movement of the critical pole pair using single controller without capacitor current feedback (arrow indicates variation of a and b ($a = b$) from 0.5 to 1).

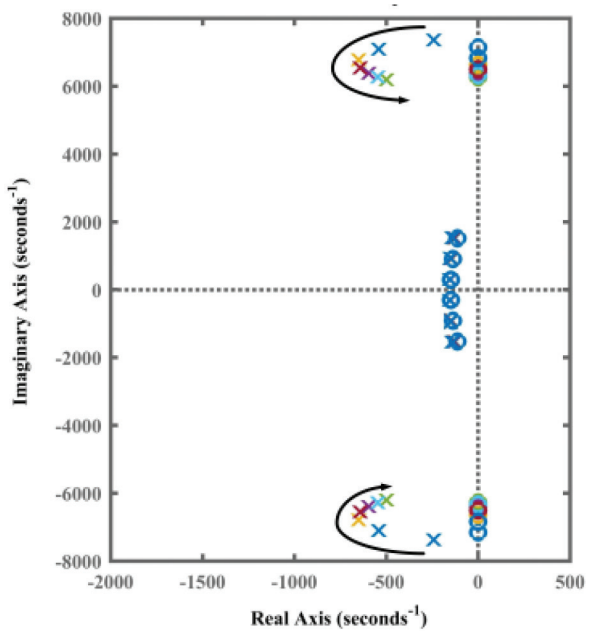

Fig. 14. Pole Zero plot depicting movement of the critical pole pair using a proposed controller (arrow indicates variation of a and b, a = 0.5 to 1, b = 0.25).

plane on increasing the gain of the controller whereas, the closed loop poles of proposed controller lie on the left half of complex s-plane with the increasing value of gain as shown in Figure 14. Figure 15 shows the performance of both controllers in bode plots when the grid side inductance is increased by 1 mH. As aforementioned, the system is unstable for higher controller gain when single controller (without capacitor feedback) is used, whereas, the proposed controller when implemented gives closed-loop stability. Hence, a higher dynamic response can be

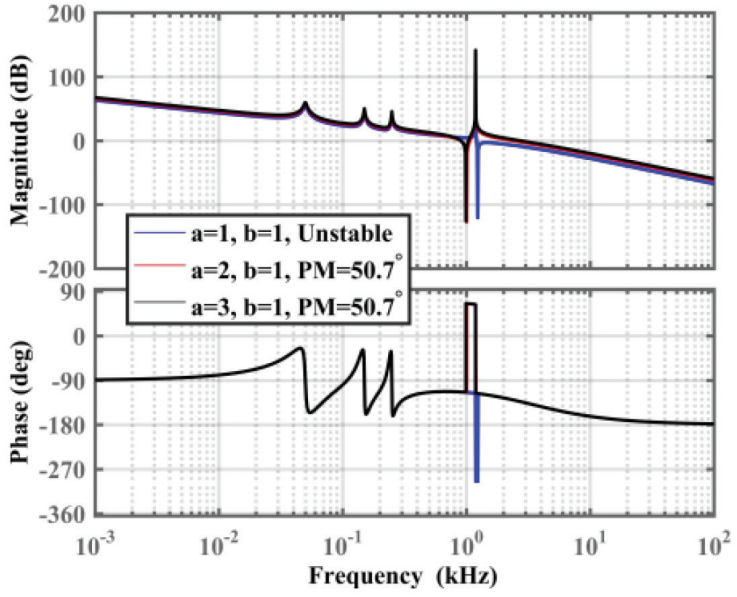

Fig. 15. Closed loop response for increased grid inductance by single ($a = b$) and proposed controller ($a \neq b$).

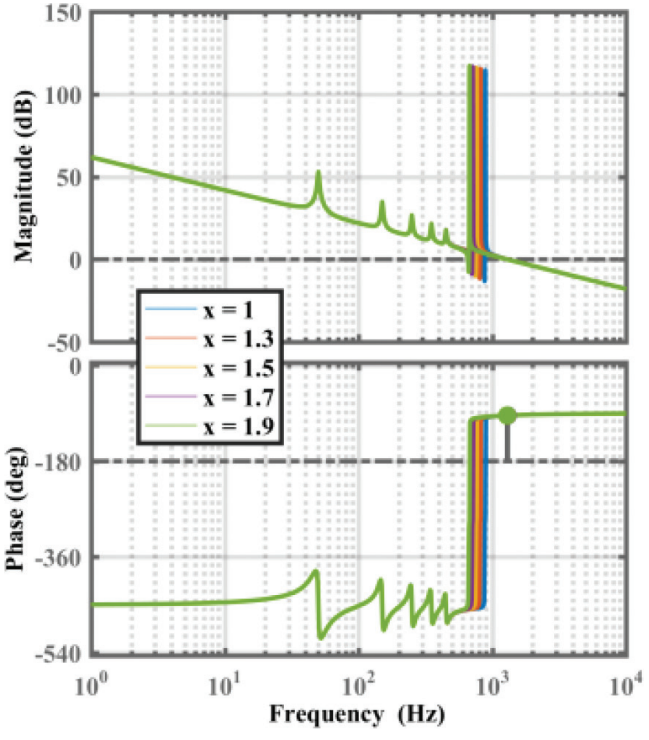

Fig. 16. Performance of the proposed system with grid inductance variation (Bode plot).

achieved with the proposed controller and it has two degrees of freedom in the controller design (*a* and *b*) to ensure a desired controller performance. Figure 16 shows bode diagram indicating the performance of the proposed controller for various series inductance values. The system is stable and gives approximately the same bandwidth when the series inductance is varied. In this figure, $x = 1$ denotes that there are no additional inductances added in the grid side and $x = 1.3$ indicates that 30% additional inductance is added. The movement of poles and zeros for

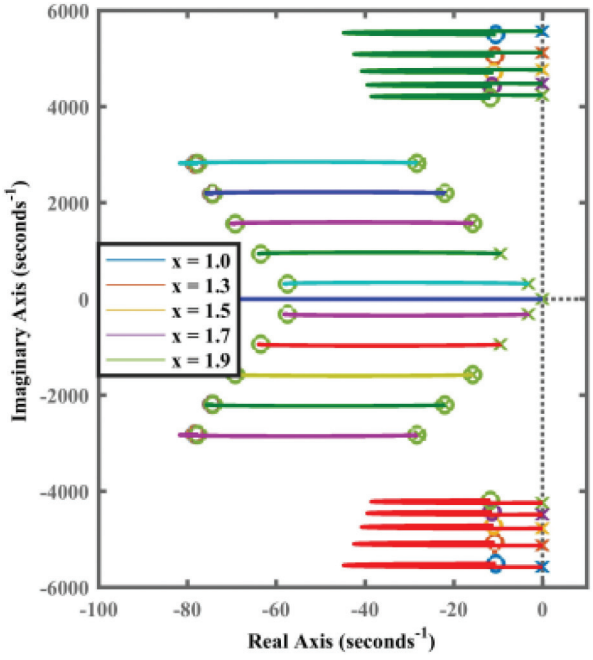

Fig. 17. Performance of the proposed system with grid inductance variation (Pole-Zero map).

the same is shown in Figure 17. A comparison with a few other control techniques reported by Hong et al. (2022) for active filter current control is provided in Table 2. In Table 2, single controller with PI controller is replaced by various controller configurations for active filtering application and all of them require additional current sensor for achieving active damping.

3. Experimental Results

The validation of the above analysis and proposed methodology that can operate the active filter at reduced PV voltage has been done by a 1.5 kW prototype. The photograph of the experimental set-up is given in Figure 18. An 80 V DC bus voltage is integrated to a 100 V RMS grid to compensate the harmonic loading.

Assuming, $V_1 = V_2$ and the turns-ratio to be 0.8 and considering various drops in the system, a DC voltage of 80 V is obtained. The values of various other elements used to achieve the objective are shown in Table 3. TMS320F28379D TI controller board is used for the purpose of closed-loop control and generating the modulation signals to the two inverters. Two LA−55P current sensors are used for sensing the load current and the shunt inverter current. Two LV−25P voltage sensors are used to sense grid voltage and DC-link voltage.

Figures 19–24 show the experimental results. Figure 19 shows the unity power factor grid, series inverter current and shunt inverter current during steady state. As mentioned earlier, the series inverter current is the compensating current. Figure 20 shows the grid current tracking during turn-on in α−β domain. The series inverter provides the harmonic component of load immediately after turn on. Hence, the grid is operated at unity power factor. Figure 21 shows the various voltage waveforms in the prototype. It can be observed that the KVL is satisfied that is, V_{grid} minus $V_{transformer}$ is equal to Vc. The grid voltage is 100 V r.m.s. whereas the DC link voltage is 80 V. Figure 22 shows the effect of increasing the grid side inductance by 1 mH. A single controller without any active damping is unable to dampen the oscillations. However, when the proposed controller is switched on the oscillations are suppressed.

Figure 23 shows the grid current during the turn-on of the load from no load to full load using an activation signal. Clearly, the grid is at unity power factor immediately after turn-on of the load. Figure 24 shows the THD level of the grid current obtained using the experimental setup. When the controller is not switched on, the THD level is 36.76%.

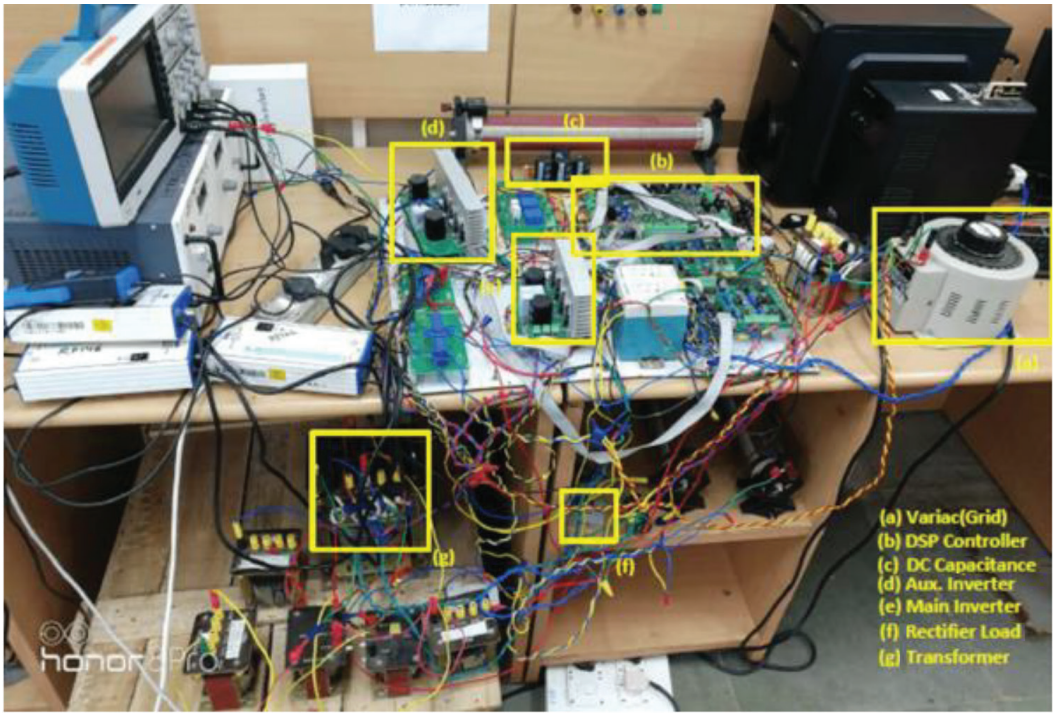

Fig. 18. Photograph of experimental setup, (a) AC Grid, (b) Controller TI TMS320F28379D, (c) DC link Capacitor, (d) Auxiliary Inverter, (e) Main Inverter, (f) Rectifier Load, (g) Transformer.

Parameter	Simulation values	Experimental values
Grid voltage	230 V RMS, 50 Hz	100 V RMS, 50 Hz
Inverter DC bus voltage	160 V	80 V
Inverter current rating	15 A	15 A
Shunt inductance	2 mH	1 mH
Series inductance	3 mH	2 mH
Series capacitance	30 μF	30 μF
Transformer turns ratio	0.8	0.8

Table 3. Power circuit parameters.

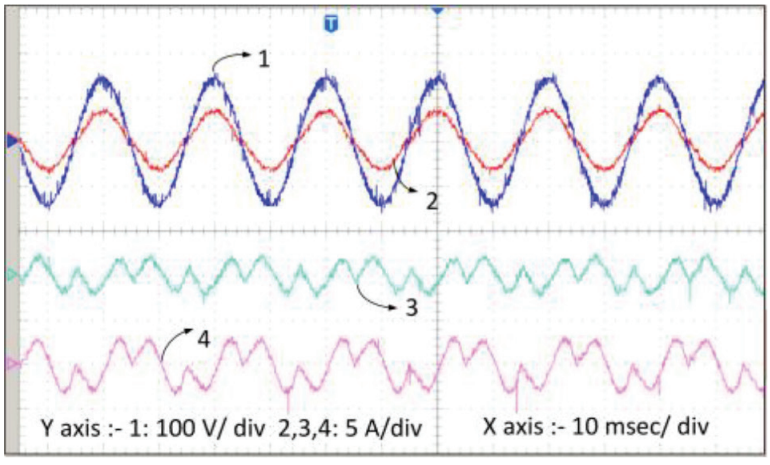

Fig. 19. Various waveforms during steady state (1 – Grid Voltage, 2 – Grid Current, 3 – Series Inverter Current, 4 – Shunt Inverter Current).

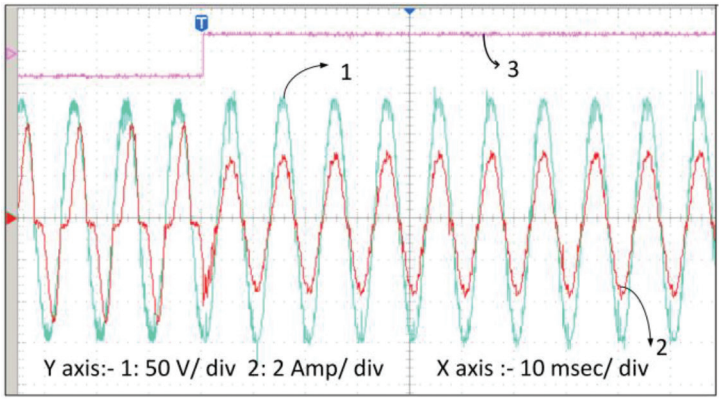

Fig. 20. Grid voltage and grid current during turn-on of the controller (1 – Grid Voltage, 2 – Grid Current).

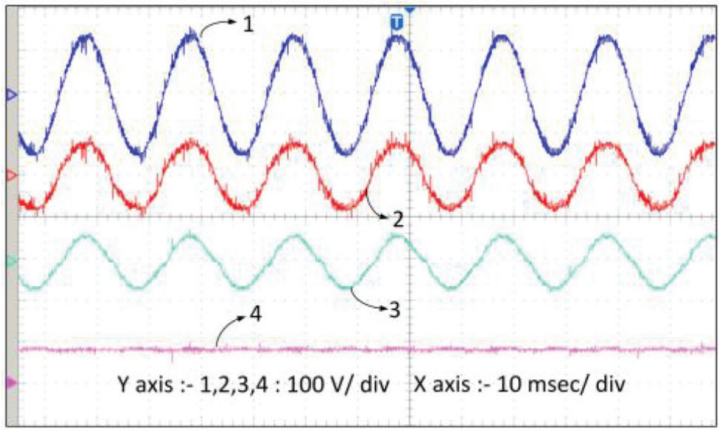

Fig. 21. Grid voltage, transformer voltage and capacitor voltage satisfying KVL equation and the DC bus voltage (1 – Grid Voltage, 2 – Transformer Voltage, 3 – Capacitor Voltage, 4 – DC bus Voltage).

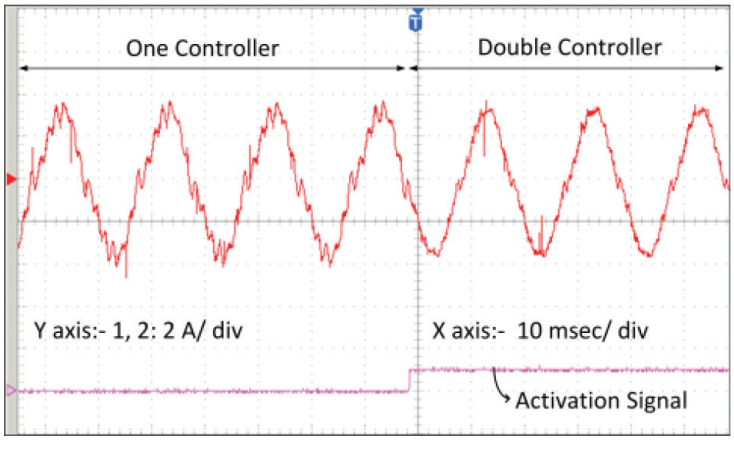

Fig. 22. Grid current during transient from single controller to proposed controller.

When the proposed controller is switched on, the grid current THD reduces to 7.2%. On the other hand, the single controller is able to reduce the grid THD level to 14.27%. The THD from third harmonic onwards is zoomed and shown as an inset.

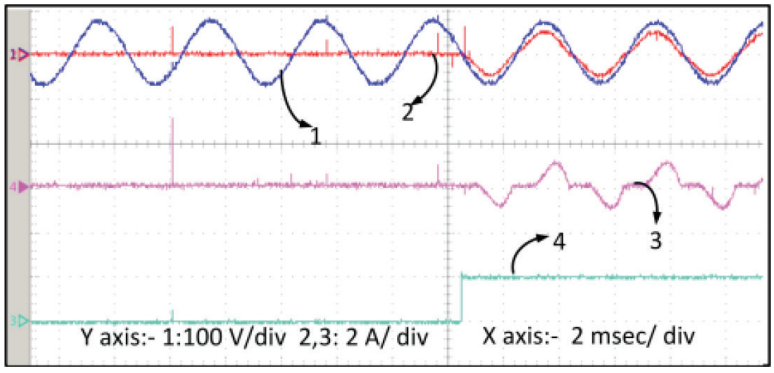

Fig. 23. Grid voltage, grid current during load turn on (1 – Grid Current, 2 – Grid Voltage, 3 – Load Current, 4 – Activation Signal).

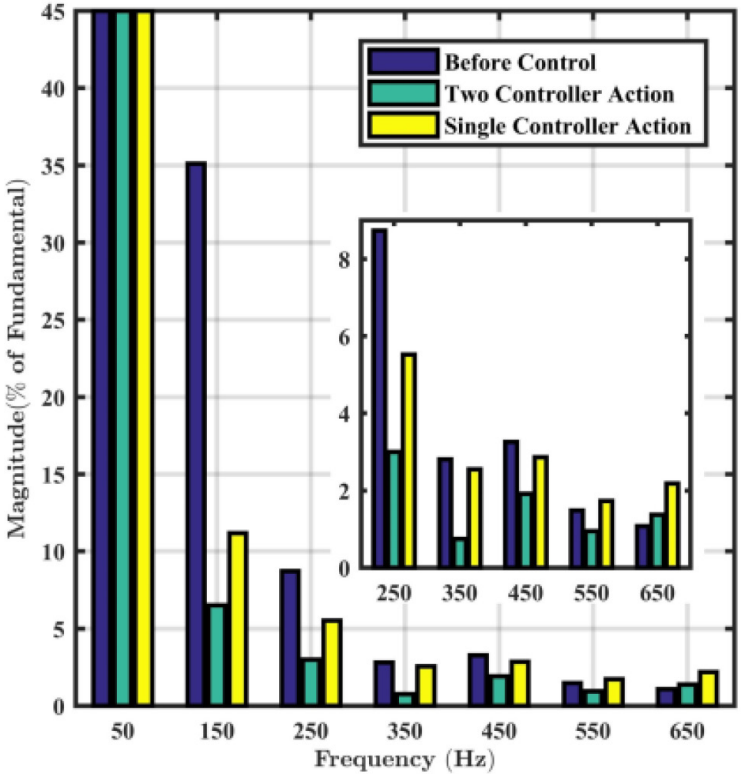

Fig. 24. Grid current THD before control action, after two controller actions and after single controller action (Experimental).

4. Simulation Results

The THD analysis of grid current in the system described above is shown in Figure 25. The system parameters are mentioned in Table 3. The grid current THD before and after controller action is compared. Two control action reduces the grid THD from 46% to 3.83% whereas, the grid THD is 6.79% by single controller action with reduced controller gain. Owing to the reduced controller gain, the grid current THD in case of single controller action is higher.

Figure 26 shows the operation of the system using one controller and two controllers after increasing grid inductance by 1 mH. At t = 0.25 s, single controller is switched on. Upon increasing the value of controller gain,

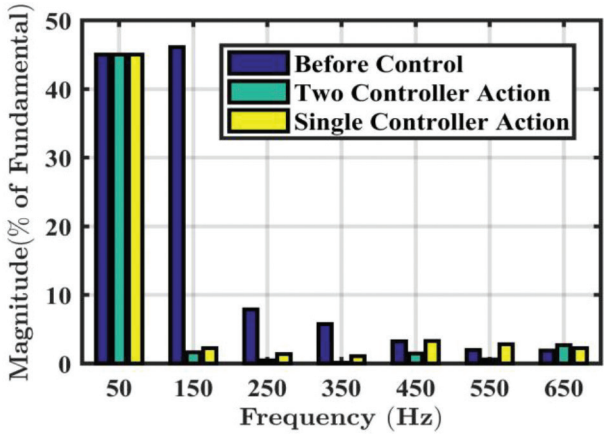

Fig. 25. Grid Current THD using proposed two controllers (Simulation).

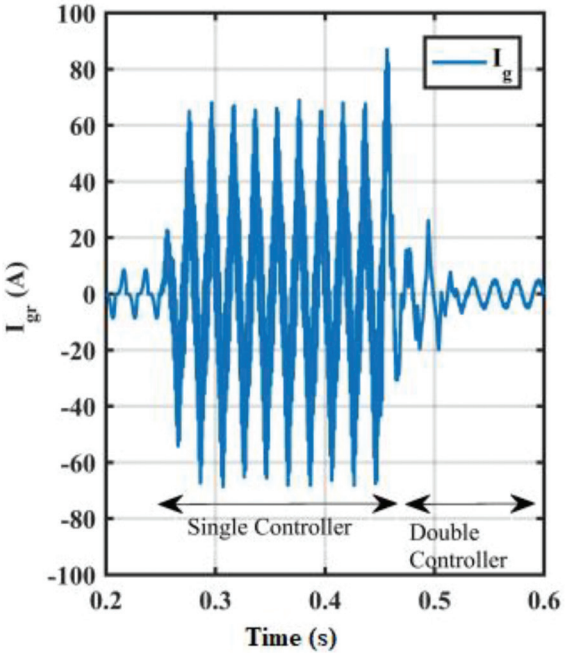

Fig. 26. Grid Current during one controller and two controller action.

Grid inductance	THD using proposed controller (%)
1 mH	3.40
2 mH	3.24
3 mH	3.51

Table 4. Grid current THD for various grid inductances.

system oscillations are set in because of the instability of the controller. At t = 0.45 s two controller is switched on. It can be observed that one controller operation results in system oscillations whereas two controller restores the system to normalcy. The THD of the grid current for various grid inductance using the proposed controller using the controller parameters given in Table 5 is shown in Table 4. Since the implementation of single controller gives instability issues, the THD values are not mentioned.

Controller parameters	Simulation studies	Experimental studies
ζ	0.02	0.02
K_p for P_1	0.03 A^{-1}	0.03 A^{-1}
K_p for P_2	0.04 A^{-1}	0.04 A^{-1}
K_{i1} for P_1	17 rad A^{-1} s^{-1}	17 rad A^{-1} s^{-1}
K_{i3} for P_1	19 rad A^{-1} s^{-1}	19 rad A^{-1} s^{-1}
K_{i5} for P_1	24 rad A^{-1} s^{-1}	24 rad A^{-1} s^{-1}
K_{i7} for P_1	30 rad A^{-1} s^{-1}	30 rad A^{-1} s^{-1}
K_{i9} for P_1	38 rad A^{-1} s^{-1}	38 rad A^{-1} s^{-1}
K_{i1} for P_2	22 rad A^{-1} s^{-1}	22 rad A^{-1} s^{-1}
K_{i3} for P_2	22 rad A^{-1} s^{-1}	22 rad A^{-1} s^{-1}
K_{i5} for P_2	22 rad A^{-1} s^{-1}	22 rad A^{-1} s^{-1}
K_{i7} for P_2	22 rad A^{-1} s^{-1}	22 rad A^{-1} s^{-1}
K_{i9} for P_2	22 rad A^{-1} s^{-1}	22 rad A^{-1} s^{-1}

Table 5. Control circuit parameters.

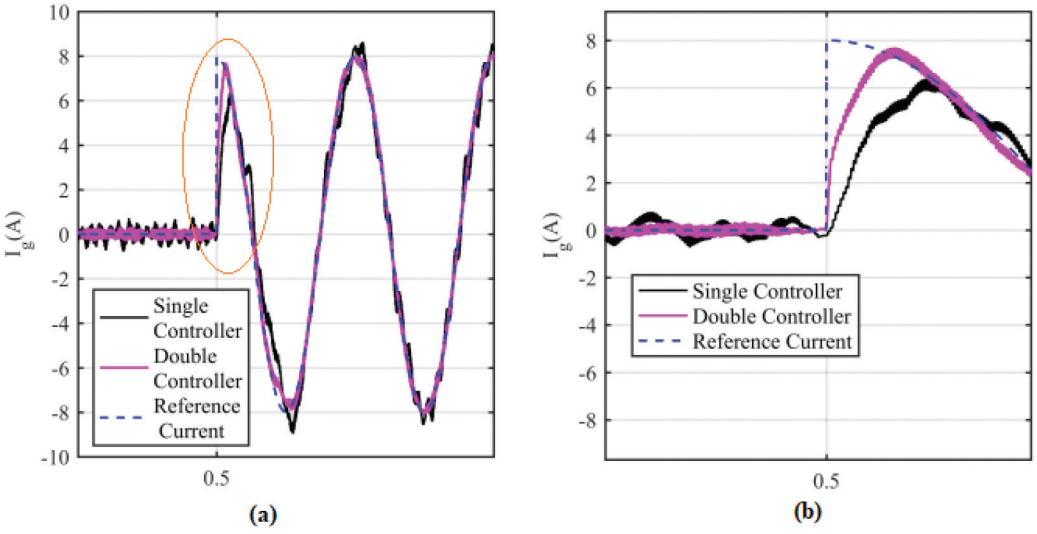

Fig. 27. (a) Injection of reference current to grid; (b) Zoomed image of the encircled portion.

Figure 27(a) shows the transient response of both controllers by injecting a reference current to the grid. Figure 27(b) gives the zoomed image of Figure 27(a). The rise time in case of single controller is more than that of the proposed controller. Also, the oscillation tendency can be observed with slight increase in the controller gain when single controller is used. The proposed controller tracks the reference current precisely.

5. Conclusion

This paper presents a new power converter configuration for reduced DC voltage using series voltage injection along with a novel control scheme. The DC voltage reduction is achieved via series-shunt combination of converter along with a reduced kVA rating transformer. The paper proposes a two controller with single feedback parameter that is one of the two converter currents for the purpose of active filtering and LCL resonance damping. The proposed controller enhances the dynamic response of the system and its performance is compared with that of the single controller case. The single controller is applicable for certain range of source inductance. However, if there is a variation in impedance, it fails to operate creating LCL based resonance. The proposed concepts are verified through simulation studies and experimental investigation. The simulation and experimental results show the

effectiveness of the proposed controller. With the proposed controller, an improved grid THD is obtained compared to single controller with reduced DC bus operation. The future work includes the extension of the proposed concepts to three-phase four-wires systems and to systems with grid voltages with harmonics/distortions. Two proportional multi-resonant controllers in the proposed configuration can be replaced by any other controllers (two controllers) to achieve the benefit of sensor reduction.

References

Akhavan, A., Vasquez, J. C. and Guerrero, J. M. (2021). "A Robust Stability Approach for Current-Controlled Grid-Connected Inverters Using PCC Voltage Feedforward Method," *2021 Zooming Innovation in Consumer Technologies Conference (ZINC)*, Novi Sad, Serbia, 2021, pp. 246-251. doi: 10.1109/ZINC52049.2021.9499278.

Albatran, S., Koran, A., Smadi, I. A. and Ahmad, H. J. (2018). Optimal Design of Passive RC Damped LCL Filter for Grid-Connected Voltage Source Inverters. *Electrical Engineering*, 100, pp. 2499–2508. doi: 10.1007/s00202-018-0725-5.

Almaguer, J., Cárdenas, V., Aganza-Torres, A., González, M. and Alcalá, J. (2019). A Frequency-Based LCL Filter Design and Control Considerations for Three-Phase Converters for Solid-State Transformer Applications. *Electrical Engineering*, 101, pp. 545–558. doi: 10.1007/s00202-019-00801-0.

Barva, A. V. and Joshi, S. (2022). A comprehensive survey on hybrid active power filter topologies & controller and application in Microgrid. In: *2022 IEEE Region 10 Symposium (TENSYMP)*, 01–03 July 2022. Mumbai, India: IEEE, pp. 1–6. doi: 10.1109/TENSYMP54529.2022.9864377.

Behera, R. R., Dash, A. R. and Panda, A. K. (2021). Cascaded Transformer coupled Multi-level inverter based Shunt Active Power Filter. In: *2021 Asian Conference on Innovation in Technology (ASIANCON)*, 27–29 August 2021. Pune, India: IEEE, pp. 1–6. doi: 10.1109/ASIANCON51346.2021.9544884.

Bhattacharya, A., Chakraborty, C. and Bhattacharya, S. (2012). Parallel-Connected Shunt Hybrid Active Power Filters Operating at Different Switching Frequencies for Improved Performance. *IEEE Transactions on Industrial Electronics*, 59(11), pp. 4007–4019. doi: 10.1109/TIE.2011.2173893.

Buyuk, M., Tan, A. and Tumay, M. (2018). Improved Adaptive Notch Filter-Based Active Damping Method for Shunt Active Power Filter with LCL-Filter. *Electrical Engineering*, 100, pp. 2037–2049. doi: 10.1007/s00202-018-0685-9.

Gajjar, N. A. and Zaveri, T. N. (2018). A review of D-STATCOM used in solar photovoltaic system. In: *2018 International Conference and Utility Exhibition on Green Energy for Sustainable Development (ICUE)*, 24–26 October 2018. Phuket, Thailand: IEEE, pp. 1–7. doi: 10.23919/ICUE-GESD.2018.8635787.

Gao, L., Dougal, R. A., Liu, S. and Lotova, A. P. (2009). Parallel-Connected Solar PV System to Address Partial and Rapidly Fluctuating Shadow Conditions. *IEEE Transactions on Industrial Electronics*, 56(5), p. 2009. doi: 10.1109/TIE.2008.2011296.

Gonzalez, J. M., Busada, C. A. and Solsona, J. A. (2021). A Robust Controller for a Grid-Tied Inverter Connected through an LCL Filter. *IEEE Journal of Emerging and Selected Topics in Industrial Electronics*, 2(1), pp. 82–89. doi: 10.1109/JESTIE.2020.3014834.

Hong, Q.-R., Sou, W.-K., Chan, P.-I., Gong, C. and Lam, C.-S. (2022). Review of different current control strategies for LC-coupling hybrid active power filter. In: *IECON 2022 – 48th Annual Conference of the IEEE Industrial Electronics Society*, 17–20 October 2022. Brussels, Belgium: IEEE, pp. 1–6. doi: 10.1109/IECON49645.2022.9968561.

Jeong, H., Lee, K., Choi, S. and Choi, W. (2010). Performance Improvement of LCL-Filter-Based Grid-Connected Inverters using PQR Power Transformation. *IEEE Transactions on Power Electronics*, 25(5), pp. 1320–1330. doi: 10.1109/TPEL.2009.2037225.

Johnsana, J. S. L. and Kumar, R. S. (2022). A new shunt hybrid active power filter configuration research and implementation for enhancement of power quality. In: *2022 International Conference on Computer, Power and Communications (ICCPC)*, 14–16 December. Chennai, India: IEEE, pp. 547–551. doi: 10.1109/ICCPC55978.2022.10072093.

Khenar, M., Taghvaie, A., Adabi, J. and Rezanejad, M. (2018). Multi-Level Inverter with Combined T-Type and Cross-Connected Modules. *IET Power Electronics*, 11(8), pp. 1407–1415. doi: 10.1049/iet-pel.2017.0378.

Kim, S. and Enjeti, P. N. (2002). A New Hybrid Active Power Filter (APF) Topology. *IEEE Transactions*

on Power Electronics, 17(1), pp. 48–54. doi: 10.1109/63.988669.

Luo, A., Peng, S., Wu, C., Wu, J. and Shuai, Z. (2012). Power Electronic Hybrid System for Load Balancing Compensation and Frequency-Selective Harmonic Suppression. *IEEE Transactions on Industrial Electronics*, 59(2), pp. 723–732. doi: 10.1109/TIE.2011.2161066.

Luo, A., Zhao, W., Deng, X., Shen, Z. J. and Peng, J. -C. (2009). "Dividing Frequency Control of Hybrid Active Power Filter With Multi-Injection Branches Using Improved *ip--iq* Algorithm," in *IEEE Transactions on Power Electronics*, 24(10), pp. 2396-2405. doi: 10.1109/TPEL.2009.2019822.

Mondol, M. H., Biswas, S. P. and Hosain, M. K. (2022). A New Magnetic Linked Three Phase Multi-level Inverter with Reduced Number of Switches and Balanced DC Sources. *Electrical Engineering*, 104, pp. 449–461. doi: 10.1007/s00202-021-01318-1.

Naidu, P. G., Saibabu, C. and Satyanarayana, S. A. (2021). Single Phase Five-Level Inverter with Single and Multiple Switch Fault Tolerance Capabilities. *Electrical Engineering*, 103(9–3150), p. 2021. doi: 10.1007/s00202-021-01295-5.

Nikam, D. S. and Kalkhambkar, V. N. (2018). STATCOM and multilevel VSC topology: A review. In: *2018 International Conference on Current Trends towards Converging Technologies (ICCTCT)*. Coimbatore, India: IEEE, pp. 1–7. doi: 10.1109/ICCTCT.2018.8551170.

Olalla, C., Clement, D., Rodriguez, M. and Maksimovic, D. (2013). Architectures and Control of Submodule Integrated DC-DC Converters for Photovoltaic Applications. *IEEE Transactions on Power Electronics*, 28(6), pp. 2980–2997. doi: 10.1109/TPEL.2012.2219073.

Pan, D., Ruan, X., Bao, C., Li, W. and Wang, X. (2014). Capacitor-Current Feedback Active Damping with Reduced Computation Delay for Improving Robustness of LCL-Type Grid-Connected Inverter. *IEEE Transactions on Power Electronics*, 29(7), pp. 3414–3427. doi: 10.1109/TPEL.2013.2279206.

Park, S., Sung, J. H. and Nam, K. (1999). A new parallel hybrid filter configuration minimizing active filter size. In: *30th Annual IEEE Power Electronics Specialists Conference. Record. (Cat. No.99CH36321)*, 01–01 July 1999. Charleston, SC, USA: IEEE, Vol. 1, pp. 400–405. doi: 10.1109/PESC.1999.789036.

Parker, S. G., McGrath, B. P. and Holmes, D. G. (2014). Regions of Active Damping Control for LCL Filters. *IEEE Transactions on Industry Applications*, 50(1), pp. 424–432. doi: 10.1109/TIA.2013.2266892.

Pea, J. C. U., Sampaio, L. P., de Brito, M. A. G. and Canesin, C. A. (2020). RLC Passive Damped LCL Single-Phase Voltage Source Inverter with Capability to Operate in Grid-Connected and Islanded Modes: Design and Control Strategy. *Electrical Engineering*, 102, pp. 2509–2519. doi: 10.1007/s00202-020-01045-z.

Pea-Alzola, R., Liserre, M., Blaabjerg, F., Sebastin, R., Dannehl, J. and Fuchs, F. W. (2014). Systematic Design of the Lead-Lag Network Method for Active Damping in LCL-Filter Based Three Phase Converters. *IEEE Transactions on Industrial Informatics*, 10(1), pp. 43–52. doi: 10.1109/TII.2013.2263506.

Pilli, N. K., Raghuram, M., Kumar, A. and Singh, S. K. (2019). Single DC-Source Based Seven-Level Boost Inverter for Electric Vehicle Application. *IET Power Electronics*, 12(13), pp. 3331–3339. doi: 10.1049/iet-pel.2019.0255.

Rahmani, S., Hamadi, A., Al-Haddad, K. and Dessaint, L. A. (2014). A Combination of Shunt Hybrid Power Filter and Thyristor-Controlled Reactor for Power Quality. *IEEE Transactions on Industrial Electronics*, 61(5), pp. 2152–2164. doi: 10.1109/TIE.2013.2272271.

Rosso, R., Wang, X., Liserre, M., Lu, X. and Engelken, S. (2021). Grid-Forming Converters: Control Approaches, Grid-Synchronization, and Future Trends—A Review. *IEEE Open Journal of Industry Applications*, 2, pp. 93–109. doi: 10.1109/OJIA.2021.3074028.

Sadanala, C., Pattnaik, S. and Singh, V. P. (2021). A Novel Switched Capacitor-Based Multi-level Inverter with Symmetrical and Asymmetrical Configurations. *Electrical Engineering*, 103, p. 14611472. doi: 10.1007/s00202-020-01172-7.

Satpathy, G., Patnaik, P. and De, D. (2017). Shunt compensation with reduced DC bus voltage using modulation margin controller. In: *2017 14th IEEE India Council International Conference (INDICON)*, 15–17 December 2017. Roorkee, India: IEEE, pp. 1–6. doi: 10.1109/INDICON.2017.8488036.

Srianthumrong, S. and Akagi, H. (2002). A medium-voltage transformerless AC/DC power conversion system consisting of a diode rectifier and a shunt hybrid filter. In: *Conference Record of the 2002 IEEE Industry Applications Conference. 37th IAS Annual Meeting (Cat. No.02CH37344)*, 2002. Pittsburgh, PA, USA, Vol. 1, pp. 78–85. doi: 10.1109/IAS.2002.1044070.

Tang, Y., Loh, P. C., Wang, P., Choo, F. H., Gao, F. and Blaabjerg, F. (2012). Generalized Design of

High Performance Shunt Active Power Filter with Output LCL Filter. *IEEE Transactions on Industrial Electronics*, 59(3), pp. 1443–1452. doi: 10.1109/TIE.2011.2167117.

Tangtheerajaroonwong, W., Hatada, T. and Akagi, H. (2007). A Transformerless Hybrid Active Filter Using a Three-Level Diode-Clamped PWM Converter. In: *2007 Power Conversion Conference – Nagoya*, 02–05 April 2007. Nagoya, Japan: IEEE, pp. 667–673. doi: 10.1109/PCCON.2007.373037.

Wang, X., Blaabjerg, F. and Loh, P. C. (2016). Grid-Current-Feedback Active Damping for LCL Resonance in Grid-Connected Voltage-Source Converters. *IEEE Transactions on Power Electronics*, 31(1), pp. 213–223. doi: 10.1109/TPEL.2015.2411851.

Wu, W., He, Y., Tang, T. and Blaabjerg, F. (2013). A New Design Method for the Passive Damped LCL and LLCL Filter-Based Single-Phase Grid-Tied Inverter. *IEEE Transactions on Industrial Electronics*, 60(10), pp. 4339–4350. doi: 10.1109/TIE.2012.2217725.

Yao, W., Yang, Y., Zhang, X., Blaabjerg, F. and Loh, P. C. (2017). Design and Analysis of Robust Active Damping for LCL Filters using Digital Notch Filters. *IEEE Transactions on Power Electronics*, 32(3), pp. 2360–2375. doi: 10.1109/TPEL.2016.2565598.

Yin, J., Duan, S. and Liu, B. (2013). Stability Analysis of Grid-Connected Inverter with LCL Filter Adopting a Digital Single-Loop Controller with Inherent Damping Characteristic. *IEEE Transactions on Industrial Informatics*, 9(2), pp. 1104–1112. doi: 10.1109/TII.2012.2222424.

Zhang, Q., Qian, L., Zhang, C. and Cartes, D. (2006). Study on grid connected inverter used in high power wind generation system. In: *Conference Record of the 2006 IEEE Industry Applications Conference Forty-First IAS Annual Meeting*, 08–12 October 2006. Tampa, FL, USA: IEEE, Vol. 2, pp. 1053–1058. doi: 10.1109/IAS.2006.256654.